Journal of Fluorine Chemistry 131 (2010) 676–683

Contents lists available at ScienceDirect

Journal of Fluorine Chemistry

journal homepage: www.elsevier.com/locate/fluor

New synthesis methods for fluorinated carbon nanofibres and applications

W. Zhang [a], L. Spinelle [a,b], M. Dubois [a,*], K. Guérin [a], H. Kharbache [c], F. Masin [c], A.P. Kharitonov [d], A. Hamwi [a], J. Brunet [b], C. Varenne [b], A. Pauly [b], P. Thomas [e], D. Himmel [e], J.L. Mansot [e]

[a] Clermont Université, UBP, Laboratoire des Matériaux Inorganiques (CNRS-UMR 6002), 24 Avenue des Landais, 63177 Aubière, France
[b] Clermont Université, UBP, Laboratoire des Sciences des Matériaux Et d'Automatique (UMR CNRS 6602), 24 Avenue des Landais, 63177 Aubière Cedex, France
[c] Matière Condensée et Résonance Magnétique, Université Libre de Bruxelles, CP 232, Boulevard du Triomphe, B-1050 Bruxelles, Belgium
[d] Institute of Energy Problems of Chemical Physics (Branch) of the Russian Academy of Sciences, Chernogolovka, Moscow Region, 142432, Russia
[e] Faculté des Sciences Exactes et Naturelles, Groupe de Technologie des Surfaces et Interfaces (GTSI), EA 2432, Université des Antilles et de la Guyane, 97159 Pointe Pitre Cedex, France

ARTICLE INFO

Article history:
Received 17 November 2009
Received in revised form 18 February 2010
Accepted 19 February 2010
Available online 11 March 2010

Keywords:
Fluorination
Carbon nanofibres
Ozonation
Tribology

ABSTRACT

Several new synthesis methods of fluorinated carbon nanofibres, such as controlled fluorination using fluorinating agent (TbF_4 or XeF_2), or assisted fluorination under UV and gamma irradiation, are reviewed and compared with the direct fluorination using undiluted fluorine gas. The results highlight the different fluorination mechanisms for the direct fluorination and the new methods. The other advantage of those alternative fluorination routes is the possibility to provide fine tuning of the fluorination level, i.e. from F/C atomic ratio close to zero, as a functionalization, to the unity (CF_1) according to the required application, electrochemical or tribological. Two applications are described in this paper as a function of the fluorine content: protection against ozonation and use as solid lubricants.

1. Introduction

Since the discovery of the carbon nanotubes by Iijima [1], their functionalization has been extensively studied. The fluorination is one of the most efficient routes to modify the physico-chemical properties of carbon materials in order to enlarge their application domain. Many applications are expected for the fluorinated carbon materials such as electrode material for primary lithium batteries [2], solid lubricants [3], or as reservoir for very strong molecular oxidizers such as BrF_3 and ClF_3 [4]. For all these applications, which cover the overall fluorine content range, i.e. the F/C atomic ratio from value close to zero (functionalization) to 1 (CF_1), the chemical, electrochemical and tribological properties depend strongly of the C–F bonding into the fluorocarbon matrix.

Up to now, the direct fluorination using pure fluorine gas remains the most useful method to obtain fluorinated carbons due to a high reactivity of molecular fluorine. This reactivity becomes a disadvantage when a given F/C fluorine content lower than the unity is required. It is then necessary to control the reactivity, using either the dilution with an inert gas (N_2, Ar) or the decrease of the reaction temperature.

In particular, for one of the most important commercial applications of fluorinated carbons, i.e. the use as positive electrode material in primary lithium batteries, the benefit of F/C lower than 1 has been underlined [5]. Nano-domains of unfluorinated carbons atoms must be present.

In order to both limit the structural defects and cover the overall fluorination level ($0.03 < F/C < 1.0$) alternative fluorination routes can be applied. In this paper, we paid our attention to the controlled fluorination using fluorinating agents (FA) (TbF_4, XeF_2) and assisted fluorination (i) by UV and γ irradiation, (ii) by ball-milling and (iii) at high F_2 pressure. Most of these methods have never been performed with graphitized carbons. The feasibility of these methods was checked in this work and the resulting samples were compared with ones obtained by direct fluorination in terms of structural defects.

Use of fluorinating agent appears as an interesting route since the kinetic of the fluorine addition to nanocarbons depends on the rate of FA thermal decomposition. The choice of the fluorinating agent is therefore a keypoint since it defines the temperature range, as well as the nature of the decomposition products (atomic or molecular fluorine). This method, called controlled fluorination, was successfully applied for the fluorination of fullerenes. Highly fluorinated fullerenes were obtained by using different fluorinating agents such as MnF_3, TbF_4, and CeF_4, etc. [6]. In this work, TbF_4 has been chosen as FA. Chilingarov et al. [7] found that its thermal decomposition into TbF_3 generates mainly atomic fluorine rather than molecular fluorine F_2. Moreover, the partial pressure of atomic fluorine is much higher than that corresponding to the equilibrium: $2F^{\bullet} \Leftrightarrow F_2$. Complementary results on the fluorination

* Corresponding author. Tel.: +33 473407105; fax: +33 473407108.
E-mail address: marc.dubois@univ-bpclermont.fr (M. Dubois).

0022-1139/$ – see front matter © 2010 Elsevier B.V. All rights reserved.
doi:10.1016/j.jfluchem.2010.02.007

with TbF_4 are discussed in the present paper in addition to the data already published [8]: tribological tests and physico-chemical characterization (high speed, 30 kHz, during the magic angle nuclear magnetic resonance experiments).

As XeF_2 decomposes into inert xenon gas and fluorine, the carbonaceous sample and the FA can be mixed contrary to other solid fluorinating agent. As a matter of fact, in a general case, when the starting material and the solid FA are mixed to favour the fluorination process, an additional separation stage is necessary. For this main advantage, XeF_2 was the second FA used in the present study and this new process was investigated.

Another prospective method is the reaction of molecular fluorine with CNFs at low temperature accompanied with an ultraviolet irradiation over the absorption band of molecular fluorine. In order to perform the process at minimum possible temperature, the influence of γ irradiation and the increase of fluorine pressure up to 3.1 atm were also studied. Finally, for similar aim, ball-milling under F_2 atmosphere was also performed allowing significant fluorination even at room temperature.

The samples obtained from these methods were characterized by high resolution ^{19}F NMR. Even for low fluorine content, this method is useful to investigate the relative amounts of C–F bonds and CF_2 groups due to its sensitivity. The covalence of C–F bondings can also be extracted. Indeed, X-ray diffraction, infrared spectroscopy are not convenient when the fluorine content is low.

2. Experimental methods

2.1. Synthesis

High purity (90%) carbon nanofibres, 2–20 μm in length, were supplied by courtesy of the MER Corporation, Tucson, Arizona. They were obtained by chemical vapor deposition (CVD) and thermally treated at 1800 °C in an argon atmosphere to enhance their graphitization degree.

Direct fluorination was carried out under a pure fluorine gas flow (1 atm) at temperatures (T_F) in between 380 to 480 °C; the fluorinated samples were noted as CNF-FT_F.

In another experiment, the initial fluorine pressure P_{F2} was increased to 2 atm at room temperature in a special reactor, the fluorination was carried out at 190 °C for 4.5 h hence P_{F2} reached a value close to 3.1 atm (CNF-HP).

For the CNF fluorination by TbF_4, a nickel closed reactor was used to preserve the defined fluorine amount released by the thermal decomposition of TbF_4. TbF_4 was synthesized from TbF_3 (Aldrich, 99.9%) in pure F_2 gas at 500 °C during 12 h. Its purity (i.e. the absence of TbF_3 and oxifluoride) was systematically checked by X-ray diffraction before each reaction. The thermogravimetric analysis of TbF_4 indicated that exactly one mole of fluorine element was released per one mole of TbF_4 between 100 and 500 °C according to the reaction

$$TbF_4(s) \xrightarrow{\Delta} TbF_3(s) + F^{\bullet} \quad (1)$$

TbF_4 appears therefore as an excellent fluorine generator for controlled fluorination.

In order to avoid an additional separation step, a double-compartment oven was used: the part containing TbF_4 was heated at 450 °C whereas CNFs were heated over 420–500 °C temperature range; the process was performed under primary vacuum in order to favour the diffusion of generated atomic fluorine. The treatment duration was equal to 12 h and the obtained samples were denoted as CNF-T_{TF}.

Starting from the solid phase, fluorination was performed using gaseous xenon difluoride (XeF_2) owing to the equilibrium $XeF_2(s) \Leftrightarrow XeF_2(g)$. In the literature, fluorination of multiwall carbon nanotubes (MWCNTs) is reported at room temperature under UV irradiation and using XeF_2 as fluorinating agent [9]. Nevertheless, only low fluorination level ($CF_{0.04}$) was achieved. Therefore, as it does under UV irradiation source, xenon difluoride could be easily decomposed into atomic fluorine according to the equation:

$$XeF_2(g) \rightarrow Xe(g) + 2F^{\bullet} \quad (2)$$

Moreover, as the vapor pressure of XeF_2 is low at room temperature (3.8 mm Hg), heating allows the XeF_2 partial pressure to be increased and the reactivity with carbon may be then improved. Xenon difluoride is a colorless solid substance at room temperature [10]. Manipulation with XeF_2 needs a dry atmosphere in order to prevent its decomposition and sublimation. A stainless steel reactor with a capacity of 100 ml was therefore used for the fluorination by XeF_2. The mixture of CNFs and XeF_2 was prepared in a glove box under argon atmosphere. The reactor was then stored at room temperature during 3 days. The sample was denoted as CNF-X.

The fluorination assisted with UV-radiation was carried out in static conditions at room temperature and the fluorine pressure was equal to 1 atm. The reaction was initiated using irradiation of XeBr eximer lamp (maximum of light was at $\lambda = 283$ nm, i.e. practically at the maximum of F_2 absorption; power density ~10 mWt cm^{-2}) during 5 h throughout a sapphire window (6 cm in diameter) beforehand installed. This irradiation favours that molecular fluorine dissociates into atomic fluorine. Another excitation source (γ radiation, Co-60) has been used with the same initial conditions. The samples issued from this fluorination method were noted CNF-UV and CNF-γ, respectively. It is to note that, without UV and γ−ray irradiation, zero weight uptake was measured after exposure to F_2 gas.

The milling process was done in a planetary mill (PM-4 model, Retsch). The jar used was especially fabricated for exposition to various atmospheres. It was made of stainless steel with 80 ml capacity. Air atmosphere inside the jar was replaced in a first step by N_2 using a continuous N_2 flux (at atmospheric pressure for half an hour) and in the second step by pure F_2 gas (continuous 1 atm F_2 flux for half an hour). The milling conditions were 300 rpm with stainless steel milling balls with a diameter of 10 mm. The milling was done for time periods of 20 min. As fluorine is consumed during the process, four additions of fluorine gas were then carried out. So, the total milling duration was equal to 1 h 20 min. The resulting sample (CNF-MF_2) was compared to fluorinated CNFs (of composition $CF_{0.47}$ denoted CNF-M0) milled in the same conditions (1 h 20 min.) under Ar atmosphere, the resulting sample was denoted CNF-MAr. Table 1 summarizes the experimental conditions and the notations. It is to note that the fluorination duration was optimized in order to obtain the highest fluorine content.

2.2. Physico-chemical characterization

NMR experiments were performed at room temperature using a Tecmag spectrometer; the working frequency for ^{19}F was equal to 470.74 MHz. A magic angle spinning (MAS) NMR probe (Bruker) operating with 2.5 mm rotor was used. For ^{19}F MAS spectra, a simple sequence was used with single $\pi/2$ pulse duration of 5.5 μs. The recycle time was equal to 5 s. ^{19}F chemical shifts were referenced to $CFCl_3$.

Nitrogen adsorption isotherms were measured at 77 K by a Micromeritics ASAP 2020 automatic apparatus. Before measurements, samples were out-gassed under secondary vacuum at 300 °C during 2 h to remove adsorbed impurities.

SEM micrographs were recorded using a Cambridge Scan 360 SEM operating at 1 kV.

Table 1
Fluorination methods and fluorination levels for selected samples obtained by weight uptake.

Process	Fluorination temperatures (°C)	Fluorination durations (h)	Fluorination levels (F/C)	Notation
F_2 (1 atm)	380–480	16	0.05–1	CNF-FT$_F$ with $380 < T_F < 480$ °C
F_2 (1 atm)	380	16	0.05	CNF-F380
F_2 (1 atm)	390	16	0.08	CNF-F390
F_2 (1 atm)	435	16	0.68	CNF-F435
F_2 (1 atm)	472	16	0.90	CNF-F472
F_2 (3.1 atm)	190	4.5	0.15	CNF-HP
TbF_4	420	12	0.12	CNF-T420
TbF_4	450	12	0.56	CNF-T450
TbF_4	480	12	0.70	CNF-T480
TbF_4	500	12	0.91	CNF-T500
XeF_2	Room temperature	72	0.06	CNF-X
F_2 + UV irradiation	Room temperature	5	0.08	CNF-UV
F_2 + γ irradiation	Room temperature	5	0.03	CNF-γ
Ball-milling in F_2 environment	Room temperature	1.33	0.30	CNF-MF$_2$
F_2 + ball-milling under Ar	Room temperature	1.33	0.47	CNF-MAr
F_2 (1 atm)	430	16	0.47	CNF-M0

2.3. Ozonation

In order to evaluate the reactivity with ozone of the samples, the gas test to check the reactivity with ozone of raw and weakly fluorinated CNFs (CNF-F390 and CNF-F405) was as follows: prior to the measurements, the samples were out-gassed for 12 h at 200 °C under primary vacuum in order to remove CO_2, H_2O, HF and O_2 molecules, which could partially cover the nanofibre surface. The samples were placed between two porous poly(tetrafluoroethylene) (PTFE) membranes (pore size: 5 μm), fixed and tightened inside the chamber using two jubilee clips. The resulting inner volume was equal to 0.88 cm^3, which was filled with the suitable active material, not in a compacted way, in order to allow the circulation of the gas flow. Since the chamber was placed in an upright position, the gas flow was introduced from bottom to top to improve the gas–solid exchange. Moreover, spacers and caps ensured the mechanical rigidity of the assembly. All the elements of the chamber, as well as the inlet and outlet pipes, were made from PTFE, to avoid undesirable adsorptions or decompositions of ozone on the inner surfaces. The experimental test bench has been specifically designed for this purpose. O_3 was supplied by a generator working at different production levels (from 300 to more than 1000 ppb). Ozone concentration was monitored by a commercial O_3 analyzer (model 49i, Thermo Electron Corporation). In order to control its concentration, ozone gas was diluted with purified air using computer-driven mass flow controllers. Air was purified by two independent active charcoal and silica gel cartridges. An UV-photometric O_3 analyzer (model 49i, Thermo Electron Corporation) monitored the gas concentration at the output of the test bench. A solenoid valve controlled by temporization allowed the measurement of transient gas concentrations in both upstream (valve off: no gas-CNFs interaction) and downstream (valve on: gas concentration at the chamber outlet) from the gas exposure chamber. In addition, since the gas analyzer works according to a specific flow rate (1.2 l min^{-1}), an additional valve acted as the exhaust or vent was inserted between the solenoid valve and the analyzers. All experiments were performed at room temperature.

To quantify the reactivity of O_3 with the samples, the gas transient concentration was monitored during consecutive cycles of exposure. The gas concentration range applied was 0–300 ppb (with 20 ppb steps) in increasing path. The upstream and downstream concentrations were sequentially measured all along this range using 1 min time resolution. During the experiments, the concentration remained constant during 2 h, whereas the solenoid valve switched every 30 min. Therefore, to evaluate the reproducibility, two upstream–downstream measurements at each concentration were carried out. In total, the experiments were about 22 h duration allowing long-term information about the reactivity. Finally, the reactivity (R in percentage) was estimated using the following formula:

$$R = 100 \times \left(\frac{C_{upstream} - C_{downstream}}{C_{upstream}} \right) \quad (3)$$

where $C_{upstream}$ and $C_{downstream}$ are the O_3 concentrations before and after the gas–carbon interaction, respectively. 100% means that all O_3 molecules react with the sample whereas the zero value is related to its inertia. The applied O_3 concentrations have been chosen because they correspond to those present in real environment's atmospheres, including the normal level (below 80 ppb), the information level (ca. 80–100 ppb) and the alert level stipulated in France (from 100 to more than 200 ppb).

2.4. Tribological tests

The tribological properties of the compounds were evaluated using an alternative ball-on-plane tribometer consisting of an AISI 52100 steel ball rubbing against an AISI 52100 steel plane on which the tested material is deposited. A normal load of 10 N is applied leading to a contact diameter of 140 μm (according to Hertz's theory) and a mean contact pressure of 0.65 GPa. The sliding speed was equal to 6 mm s^{-1}. The friction coefficient μ measured after three cycles (round trips of the ball) is considered to correspond to the intrinsic tribologic properties of the deposited film. The values recorded after 3, 25, 50, 100, 250 and 400 cycles indicated the possible evolution through structural transformations during the friction process.

For comparison, two reference samples were tested in similar conditions: UF4 graphite 1 μm in diameter granulometry and graphite fluoride, which results from its fluorination at high temperature (600 °C) for 3 h and exhibit a $(CF)_n$ structural type.

3. Results and discussion

The samples can be classified according to three criteria: (i) the fluorine content, (ii) the fluorination mechanism and (iii) the nature of the C–F bonding.

3.1. Fluorine content

Table 1 and Fig. 1 summarize the different synthesis conditions and the fluorination level for each experiment. The fluorination level (F/C) was systematically evaluated by weight uptake [6,8]. A

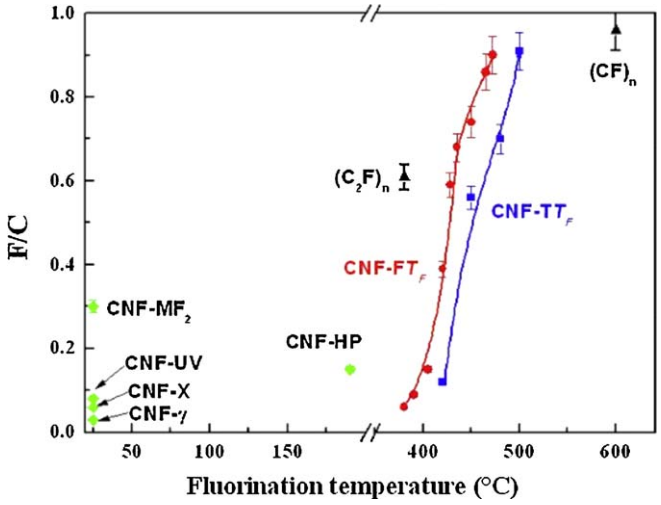

Fig. 1. F/C atomic ratio as a function of the fluorination temperature.

significant fluorination level can be reached at room temperature when the process is activated either by UV irradiation or by ball-milling. F/C is then equal to 0.08 and 0.30 for CNF-UV and CNF-MF_2, respectively. In this latter case, additional energy is provided by the friction of the ball. Nevertheless, most of the CNFs are broken and new highly reactive surfaces are formed. Grinding either in F_2 or argon atmosphere results in the mechanical breaking of the fibres. As a matter of fact, SEM images (Fig. 2) highlight that only a few residual short fibres are still present in agglomerated fluorinated carbons, namely CNF-MF_2 and CNF-MAr (see arrows in Fig. 2c and d). Nevertheless, the agglomerates appear denser when the treatment is carried out in F_2 atmosphere. Due to their tribological properties, the effects of the ball friction are slightly lowered during the grinding starting from fluorinated CNFs. Moreover, the breaking seems to occur both along and perpendicularly the fibres axis when the milling is performed under argon starting from $CF_{0.47}$ fluorinated CNFs (CNF-MAr, Fig. 2d).

Reaction temperature can be also significantly decreased by an increase of the fluorine pressure. F/C of 0.15 has been obtained at 190 °C when P_{F2} was around 3 atm. Similar fluorination level is obtained at 405 °C using 1 atm F_2 flux.

The fluorination using XeF_2 leads to a fluorination level equal to 0.06 close to the one reported by Unger et al. [9] for MWCNTs with XeF_2 under UV irradiation (F/C = 0.04). Our attempts to increase the reaction temperature up to 180 °C failed. γ irradiation under pure fluorine gas results in low F/C, equal to 0.03. These experiments indicate that, although atomic fluorine is more reactive than molecular fluorine, the fluorination at room temperature is only a surface process. Indeed, post-treatment of starting nanofibres at 1800 °C under argon atmosphere resulted in high graphitization degree, and also in high stability. For comparison, fluorination of SWCNTs using XeF_2 at 180 °C with the same process allows F/C of 0.32 to be obtained [11].

To obtain fluorination level of CNFs higher than 0.3, two methods such as controlled fluorination using TbF_4 or the direct process with F_2 gas can be applied. The F/C ratios are changed over 0.05–1 range depending on the temperature (Table 1). Due to the experimental method, the relative pressure of fluorine, atomic or molecular, is lower for the controlled method using TbF_4 than for the direct process. Hence higher reaction temperature is needed when TbF_4 is used to obtain similar fluorine content as compared with pure F_2.

3.2. Fluorination mechanism

In addition to fluorine content, the nature of the resulting fluorinated groups must be discussed. Formation of C–F bonds can be accompanied with formation of CF_2 groups on the sheet edges and on the carbon lattice structural defects. Relative amount of CF

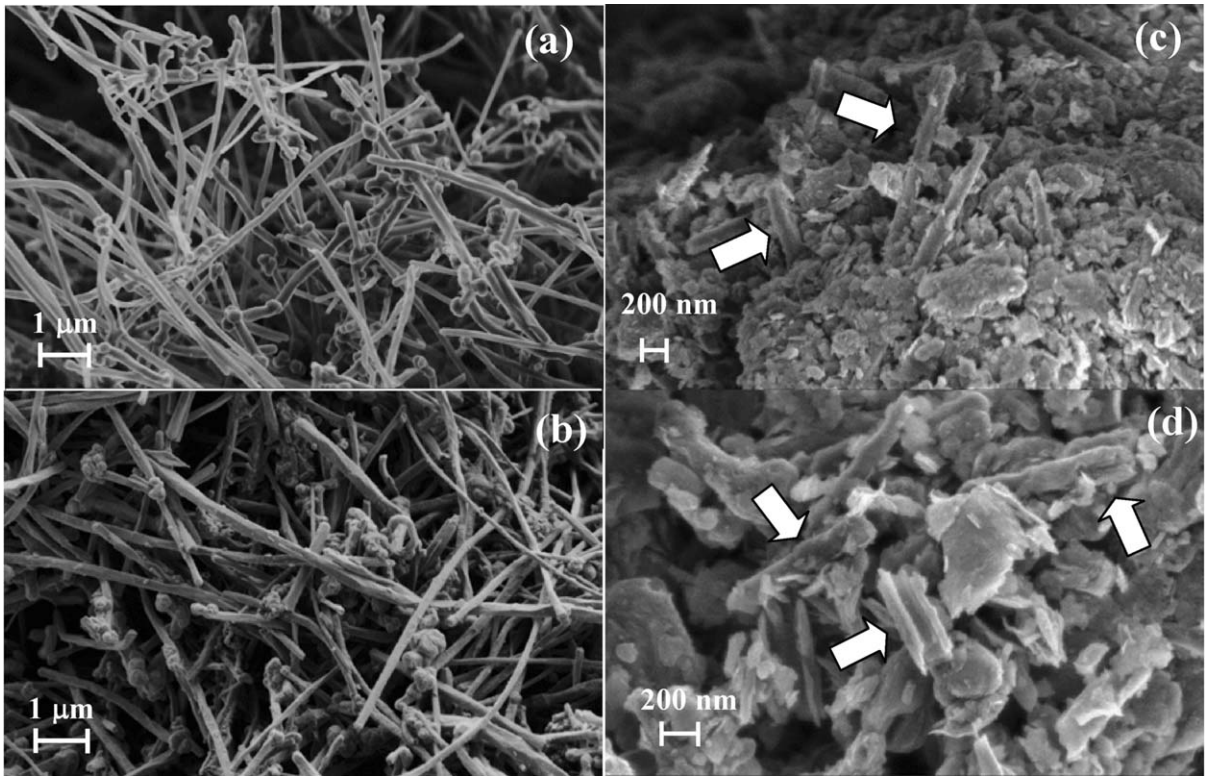

Fig. 2. SEM images of raw CNFs (a), CNF-M0 (b), CNF-MF_2 (c) and CNF-MAr (d).

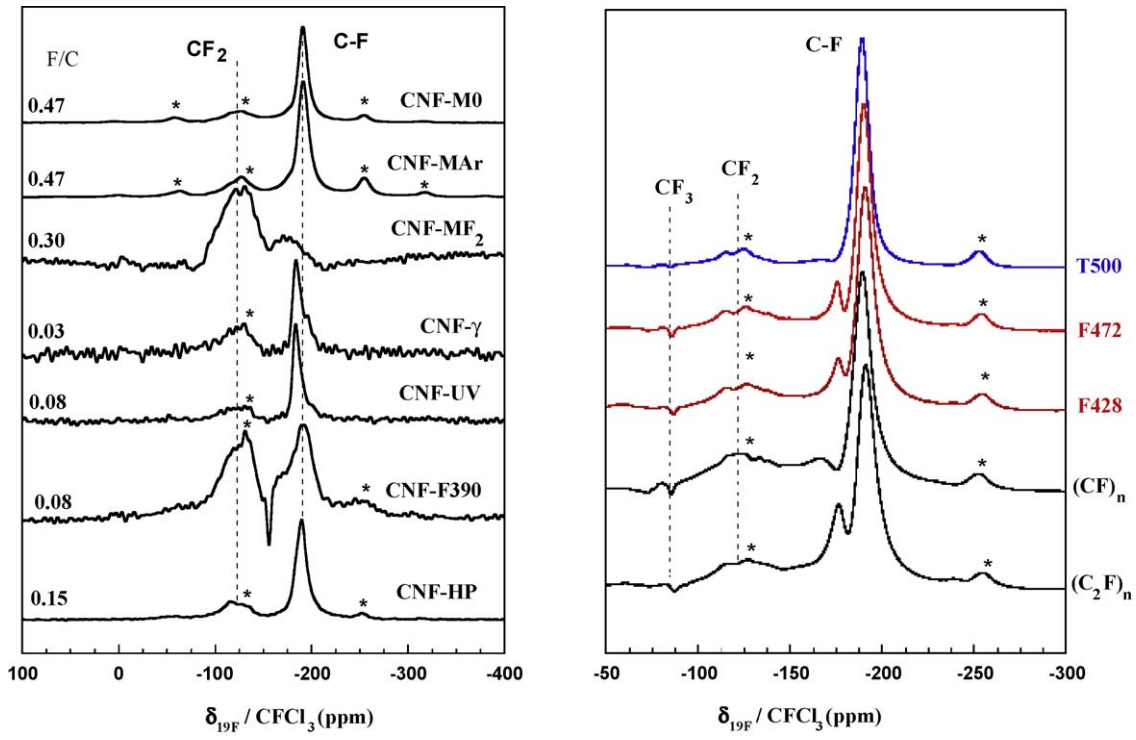

Fig. 3. ^{19}F MAS NMR spectra of fluorinated CNFs with 30 kHz spinning speed (* are the spinning sidebands); samples with low (left) and high fluorine content (right).

and CF_2 groups can be estimated from the ^{19}F NMR spectra, recorded at MAS speed of 30 kHz (Fig. 3). NMR lines are rather broad due to a strong homonuclear dipolar coupling but ^{19}F chemical shifts of CF and CF_2 covalent bonds differ sufficiently each from others (i.e. −170/−190 ppm and −120 ppm [12–16], respectively) to separate their lines. The relative amount of C–F and CF_2 will be discussed taking into account the intensities of these two lines.

As revealed by the high intensity of the corresponding NMR line, the content of CF_2 groups is the largest for CNF-MF_2 whereas the starting $CF_{0.47}$ sample and CNF-MAr exhibit mainly C–F groups. CF_2 are also predominant in CNF-γ. Both ball-milling and γ-irradiation result in structural disorder and hyperfluorination occurs for those reaction routes. The ball-milling and γ-irradiation are too energetic at this condition under F_2 atmosphere, the fluorination being effective but in majority due to CF_2 groups. Treatment with XeF_2 results also in a larger amount of CF_2 groups with respect to CF ones.

When the fluorination is performed in pure F_2 gas at high temperature ($T_F > 400$ °C) or under UV irradiation or using TbF_4, the relative amount of CF_2 groups is low. On the contrary, CNF-F390 of $CF_{0.08}$ composition exhibits a high relative amount of CF_2.

This preliminary qualitative study underlines that methods using different fluorinating agents, increase of the fluorine pressure or fluorination assisted by UV irradiation appear as promising method either to decrease the reaction temperature or to limit the structural defects as in the case of TbF_4 [8]. For low and medium fluorine contents, the C–F bonding is not strictly similar since the ^{19}F chemical shifts are equal to −182 ppm for CNF-UV and CNF-γ whereas it is equal to −190 ppm for the other sample obtained using molecular fluorine (CNF-HP, CNF-M0, CNF-MAr, CNF-MF_2, and CNF-F390). The lower the chemical shift, the higher the covalence in fluorinated carbons. The use of molecular fluorine results in slightly more covalent C–F bonding. For highly fluorinated CNFs obtained either with F_2 or TbF_4, the C–F bonding is purely covalent because the resulting ^{19}F chemical shift was equal to −190 ppm [8].

3.3. Discussion

This discussion reviews new strategies of fluorination applied to graphitized carbon nanofibres. Whereas processes using XeF_2, assisted by γ irradiation and ball-milling under F_2 gas result in a significant amount of CF_2 groups, fluorination assisted by UV irradiation, at high fluorine pressure and using TbF_4 appears as prospective alternative of the direct fluorination as concerned the decrease of the reaction temperature and/or progressiveness of the process. The difference observed between the direct fluorination and the presented methods could be due to the nature of the reactive species (molecular fluorine versus atomic fluorine generated by the thermal decomposition of TbF_4 or by dissociation of F_2 favoured under irradiation) or different ratio of atomic to molecular fluorine amount in the gaseous phase. Diffusion of $F^\bullet$ and F_2 into the carbon lattice is certainly non-equivalent. Moreover, TbF_4 decomposition allows a more progressive fluorination of the nanocarbons homogeneously dispersed through the fibre bulk as compared with the direct process using F_2 gas [8]. For the case of TbF_4, the reaction is monitored by the kinetics of FA decomposition, which provides atomic fluorine.

The comparison of samples with similar fluorination level obtained by direct and controlled fluorination using TbF_4 indicates different fluorination mechanisms. The ^{19}F NMR spectra of selected samples with spinning rate of 30 kHz are shown in Fig. 3; the spectra of covalent graphite fluorides with $(C_2F)_n$ and $(CF)_n$ structural types are added to this figure for comparison. Whatever the sample, fluorinated CNFs or graphite fluorides, the main line at −190 ppm is assigned to covalent C–F bonds [12–16]. A second line at −175 ppm is present only for CNF-F428, CNF-F472 and $(C_2F)_n$ type graphite fluoride. This line can be unambiguously assigned to fluorine nuclei present only in $(C_2F)_n$ structure: ^{19}F in weak interaction with non-fluorinated sp^3 carbon atoms. The structure of $(C_2F)_n$ can be described using a F/C/C/F stacking sequence for fluorocarbon sheets whereas for $(CF)_n$ the sequence is F/C/F/F/C/F. All carbon atoms exhibit a sp^3 hybridization. Half of the carbon atoms is fluorinated in $(C_2F)_n$ the others being linked to carbon

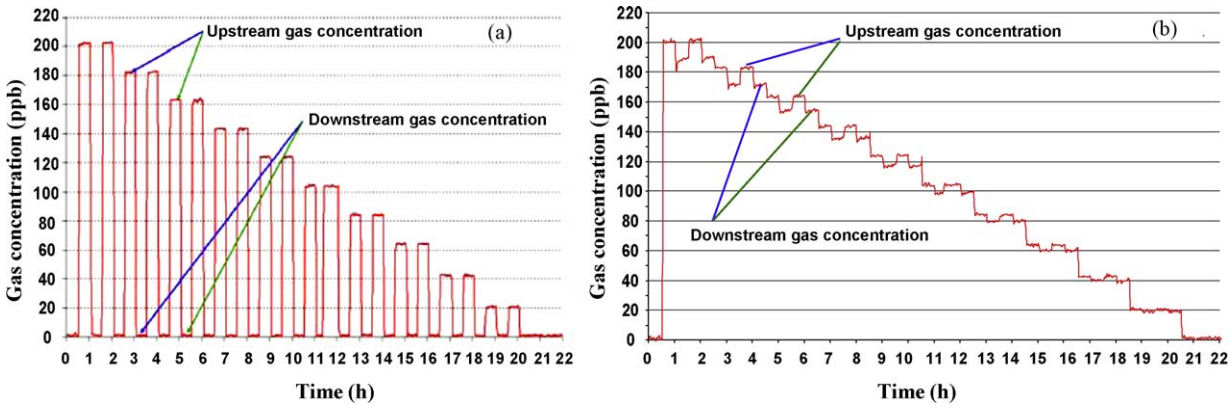

Fig. 4. Transient evolution of O_3 concentration (decreasing path) during the cycled exposure of CNFs (a) and CNF-F390 (b).

atoms. By analogy with the hyperconjugation effect in Fluorine-Graphite Intercalation Compounds (F-GICs), which involved C–C in non-fluorinated parts and C–F bonds [13,17], the covalence of the C–F bonds located close to these diamond-like atoms could be weakened in the same manner. The ^{19}F chemical shift is then of −175 ppm instead of −190 ppm for pure covalent C–F. In the case of F-GICs, −170 ppm shift is recorded. The line at −175 ppm, which is reported here for the first time due to a high spinning rate, can be considered as an indicator of the presence of $(C_2F)_n$ structural type. $(C_2F)_n$ type is formed in a wide temperature range for the direct fluorination; a temperature of 480 °C is necessary to convert it into $(CF)_n$ type, whereas $(CF)_n$ type is formed during the controlled fluorination using TbF_4 whatever the temperature. This is due to both progressive generation of atomic fluorine by thermal decomposition of TbF_4 and its high reactivity and diffusion. Indeed, the control of fluorination kinetic avoids the hyperfluorination at a high temperature. The generated atomic fluorine penetrates towards the core without formation of important structural defects. Moreover, excess of fluorine is avoided contrary to the case of a F_2 gas flux. This results in a decrease of structural defects such as CF_2, CF_3 but also dangling bonds and allows better electrochemical performances to be obtained [8].

When the fluorine content is low, the fluorination is essentially a surface process. In such a case, fluorination competes with hyperfluorination. Surface hyperfluorination means that CF_2 or CF_3 groups are formed. If this hyperfluorination continues, volatile CF_4 and C_2F_6 may be formed through a decomposition reaction. When F_2 is used at the lower temperature, at 390 °C for instance, hyperfluorination occurs and the amount of CF_2 is large (Fig. 3). On the contrary, for the case of fluorination assisted by UV irradiation, the decrease of the fluorination temperature favours the fluorination process forming C–F rather than CF_2. Atomic $F^{\bullet}$ formed by the decomposition of molecular fluorine under UV could immediately react with carbon forming C–F bonds.

In order to underline the benefits of fluorination at both low and high fluorine contents, the reaction with ozone and the tribological properties will be discussed in the following part.

4. Applications

4.1. Reactivity with ozone

Ozone reacts with a large variety of carbons, e.g. SWCNTs [18–20], activated carbons [21], through attack on the carbon and fixation of oxygen-containing groups on its surface, such as carboxylic acid, ester and quinone moieties. Using pure ozone gas, the oxidative etching of SWCNTs was even successfully used to open the end caps and the sidewalls of the nanotubes to provide access to the inner tubes [22].

The reactivity with ozone of raw and weakly fluorinated CNFs (CNF-F390 and CNF-F405) was investigated. Whatever the upstream concentration, CNFs react with almost 100% of the ozone molecules. The fluorination of CNFs, even located only on the surface, i.e. with a lower fluorine content (as low as $CF_{0.04}$), tends to terminate the reactivity. The *R* ratios are equal to 91.6, 7.0 and 4.5 for raw CNFs, CNF-F390 and CNF-F405, respectively. Fig. 4 illustrates the evolution of O_3 concentration during the consecutive and cycled O_3 gas submission throughout the upstream and downstream regimes, for the cases of raw CNFs (Fig. 4a) and the weakly fluorinated CNF-F380 (Fig. 4b). It is necessary to note that the specific surface areas are of the same order for three studied materials (i.e. 19, 16 and 30 $m^2\ g^{-1}$ for CNFs, CNF-F390 and CNF-F405, respectively, measured by the BET method with N_2 adsorption at 77 K). The decrease of reactivity means that the surface chemistry is markedly changed through the fluorination. Ozone chemically reacts with the active sites of carbon surface. The latter were saturated (oxidized) during the fluorination and the reactivity with O_3 was decreased. Fluorination appears then as a promising way to avoid the reactivity with ozone.

The combined use of ozone and activated carbons (ACs) appears as an interesting alternative to destroy toxic and poorly biodegradable molecules during wastewater treatment [23–25]. Two properties are involved: (i) a number of ACs exhibits high adsorption rate of phenolic compounds [26] and (ii) ACs are able to transform ozone into highly oxidative species in aqueous solution [27]. Both microporosity and π−π interaction between the phenolic ring and the carbon basal plane influence the adsorption of phenol, *p*-nitrophenol, and *p*-chlorophenol onto virgin granular ACs. Also, irreversible adsorption occurs through oxidative coupling reactions with basic sites on AC surface. Adsorption properties of ACs depend on both texture and surface chemistry, which may be strongly changed when it is exposed to ozone [27,28]. During ozonation treatment, adsorption properties are worsened because of the formation of carboxylic surface oxygenated groups, which favour the adsorption towards water, resulting in a lowering of π−π interactions, and prevent an irreversible adsorption [28]. Being applied to adequate carbonaceous materials, low fluorination appears as an interesting way to reduce the amount of carboxylic surface oxygenated groups prior to wastewater treatment by ozone. This treatment, which also results in increased hydrophobic character, must occur without significant change of the specific surface area in order to maintain the π−π interaction between the phenolic ring and carbon surface.

4.2. Friction properties

The analysis of the electrochemical performances indicates systematically better electrochemical behaviour of CNFs fluori-

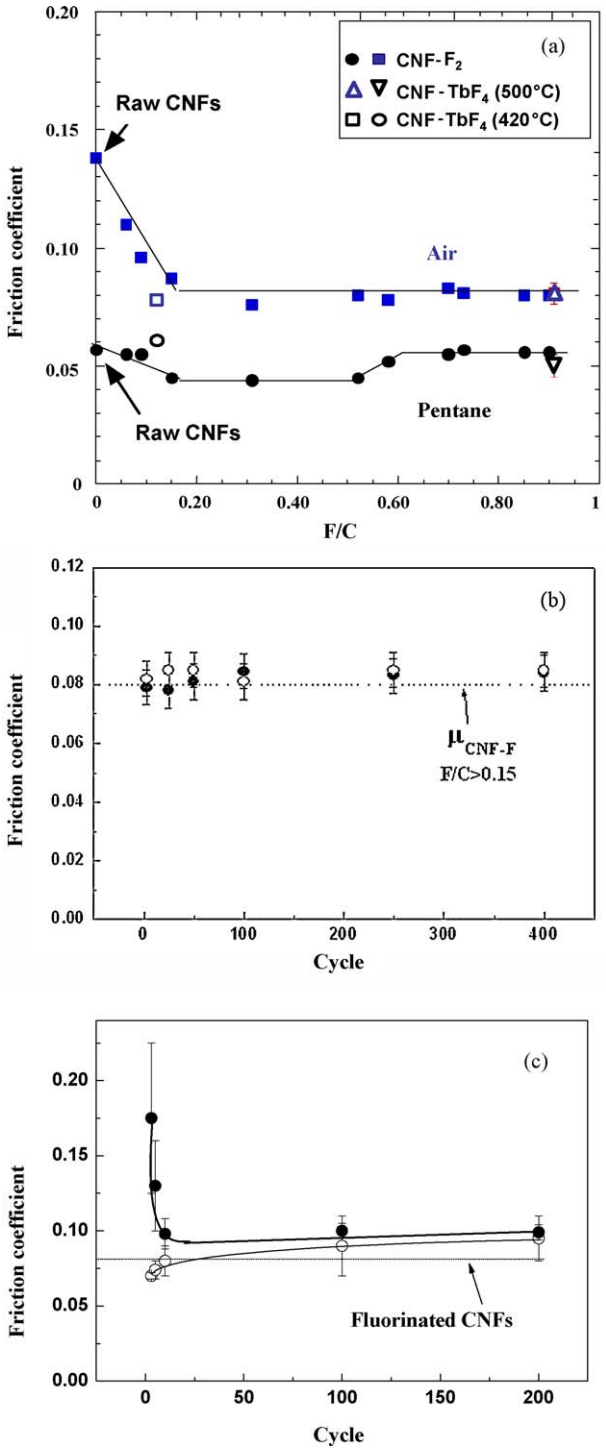

Fig. 5. (a) Evolution of friction coefficient obtained at the third cycle of CNFs fluorinated either by direct fluorination or controlled fluorination as a function of the fluorination level in pentane and air atmosphere. (b) Evolution of friction coefficient as a function of cycles number for CNF-T420 (●) and CNF-T500 (○). The friction coefficients were measured at 3, 25, 50, 100, 250 and 400 cycles. Data for CNFs fluorinated using F_2 with F/C > 0.15 are also reported (dashed line). (c) Friction coefficients upon cycling for UF4 graphite (●) and high temperature graphite fluoride of $(CF)_n$ structural type (○).

nated by the controlled fluorination. It is due to the lower amount of structural defects presented in the fluorinated CNFs obtained by TbF_4-based method [8,29]. On the contrary, tribological properties are practically independent on the fluorination method (Fig. 5). Investigations of the friction properties of pristine and fluorinated carbon nanofibres indicated a beneficial influence of fluorination on the lubricating performances of the compounds [30].

The evolutions of the friction coefficients in the presence of liquid pentane and in air for CNFs fluorinated either by direct or by controlled fluorination are presented in Fig. 5a. Whatever the fluorination method for fluorination level higher than 0.15, the friction coefficient is about the same as a function of the fluorination level. This means that no effect of the structure type, $(CF)_n$ or $(C_2F)_n$, of the fluorinated phase, is registered. Either controlled or direct process can be used for fluorination of carbon nanolubricants.

Fig. 5b presents the evolution of the friction coefficients μ of CNF-T420 and CNF-T500 as a function of cycle number. The reported friction coefficient values were measured after 3, 25, 50, 100, 250 and 500 cycles. The tribological experiments exhibit a noticeable stability of the performances for the two samples. In particular, the good friction properties are observed just from the start of the tribologic tests without any induction period to form the tribofilm. The obtained friction coefficients, close to 0.08, are nearly similar to CNFs fluorinated using F_2 gas when the F/C molar ratio is above 0.15 [30]. Such friction coefficient values are as low as those of conventional fluorocarbon lubricants [3,31–33]. For example, the friction coefficients of graphite fluoride $(CF)_n$ with $CF_{1.12}$ composition is ranged in between 0.03 and 0.15 over the 25–250 °C temperature range. Low friction coefficients, over 0.055–0.07 range and stable upon cycling, have been obtained using graphite fluoride prepared at low temperature by F_2/HF/IF_5 catalytic gaseous mixture treatment followed by post-treatment under fluorine gas at 300 °C [33]. For such compounds the optimization of the tribologic properties is related to the partial conservation of the planar shape of graphene planes. The post-treatment of initial graphite fluorides by fluorine gas at temperatures above 450 °C leads to the evolution of C–F bonding to purely covalent character resulting in puckered fluorocarbon layers formation. The increase of μ up to 0.1 is attributed to the increase of the volume fraction of puckered fluorocarbon domains.

The tubular shape of nanofibres allows improved tribological properties to be achieved in comparison with graphite and conventional $(CF)_n$ type high temperature graphite fluoride. As a matter of fact, these properties were evaluated with similar experimental conditions and the results are shown in Fig. 5c. Graphite fluoride with F/C ratio close to the unity and $(CF)_n$ structural type was synthesized by pure F_2 gas treatment at 600 °C during 3 h. Its friction coefficient is initially low but continuously increases. On the contrary, for the case of UF4 graphite several cycles are necessary to reach the lower friction coefficient. Fluorinated CNFs with F/C higher than 0.15, synthesized using either F_2 or TbF_4, exhibit low and stable friction coefficient as soon as the third cycles. Moreover, similar characteristics in terms of stability and low values have been already obtained in the case of room temperature graphite fluoride post-treated under F_2 gas but the one-step synthesis used for fluorinated CNFs appears easier than the two-step fluorination.

For the case of nanofibres, the friction reduction created by fluorination is related to the decrease of the surface free energy of fluorinated CNFs resulting from the fluorination of the first external graphene layers. This leads to the lowering of interfibres interactions. The optimum fluorination level needed to minimize the surface free energy is F/C equal to 0.15 corresponding apparently to four fluorinated layers. For fluorine contents above 0.15, the fluorination of the nanofibres internal layers does not significantly affect the surface free energy resulting in a stability of the interfibres interactions and then of the friction coefficient. Low friction coefficients obtained for CNFs fluorinated using the conventional and TbF_4-based methods when F/C > 0.15 indicate that fluorinated carbon nanofibres exhibit adequate properties to

be used as solid lubricants as well as additives in conventional liquid lubricants. For this latter case, the protective tribofilm is built on the sliding surfaces in the physical conditions of the sliding interface by the nanofibres without any chemical reactions with the substrates.

To go further to the decrease of the friction coefficient, the easier way is the modification of the environmental conditions for tribological uses. Indeed, even if the evolution of the friction coefficient as a function of the fluorination level in the two environmental conditions, air or pentane, are about the same, a significant lowering of the friction coefficient value is obtained when pentane is used instead of air (Fig. 5a). Friction coefficient values as low as 0.04 has been obtained for fluorination level ranged between 0.20 and 0.60 in pentane environment whereas the lowest friction coefficient in air was equal to 0.08. Such low values in pentane environment are due to the decrease of the surface free energy of fluorinated CNFs. Moreover, the presence of liquid in the contact zone favours interfibres sliding phenomena. The lowering of the interfibres interactions is obtained for CNFs fluorinated with F/C over 0.20–0.60 range, i.e. when fluorination has efficiently structured the CNFs surface without partial exfoliation. Complementary, it must be noticed that the friction coefficient of fluorinated CNFs is remarkably stable from the third cycle to the 160th one in various experimental environments [30].

5. Conclusion

The alternative fluorination methods presented in this paper may be complementary to the direct process using F_2 gas. As a matter of fact, when the application needs a very low amount of structural defects, for instance the use as electrode material in primary lithium battery, the controlled method using TbF_4 can be chosen. On the contrary, for use as solid lubricants, the carbon nanofibres can be fluorinated either by the controlled method using TbF_4 or the direct process, the phenomena being independent of the synthesis. So the direct fluorination as an easier route can be preferred. For tribology, the phenomena are interfacial and the only restriction is as follows: fluorine content x in CF_x should be higher than 0.15.

The case of nanofibres well illustrates the reactivity with respect to fluorine of graphitized carbonaceous nanomaterials. Due to the graphitization, high temperature is necessary to obtain high fluorine content using either TbF_4 or F_2. For the other alternative methods, fluorination results in a lower fluorine content (assisted by high F_2 pressure, mall-milling under F_2 atmosphere) or very low F/C (assisted by UV and γ-ray irradiation, method using XeF_2). These methods should be effective for more reactive materials, such as single walled carbon nanotubes.

In the case of CNFs, among the various methods, TbF_4-based fluorination and UV-irradiation assisted one must be retained because the latter allows surface fluorination with mainly C–F bonds rather than CF_2 contrary to the direct process with F_2. Due to the higher reactivity and diffusivity of atomic fluorine into the fluorocarbon matrix of atomic fluorine, use of TbF_4 results in both the exclusive formation of the highly fluorinated phase, i.e. $(CF)_n$, and the decrease of the structural disorder.

In addition to electrochemical application in primary lithium battery described elsewhere [5], two examples of possible applications for fluorinated nanofibres are presented: (i) the functionalization of the surface (F/C∼ 0.04) to protect from reactivity with ozone in wastewater treatment and (ii) utilization as solid lubricants when the fluorine content is greater than abovementioned. Very wide range of fluorine content is covered for various applications of fluorinated carbon nanofibres. Moreover, the fluorination method can be chosen in order to tune the fluorine content as a function of the application.

References

[1] S. Iijima, Nature 354 (1991) 56–58.
[2] N. Watanabe, T. Nakajima, H. Touhara, Graphite Fluorides, Amsterdam, Elsevier, 1988.
[3] R.L. Fusaro, H.E. Sliney, ASLE Trans. 13 (1970) 56–65.
[4] A.S. Nazarov, V.G. Makotchenko, Inorg. Mater. 38 (2002) 278.
[5] R. Yazami, A. Hamwi, K. Guérin, M. Dubois, Y. Ozawa, J. Giraudet, F. Masin, Electrochem. Commun. 9 (2007) 1850–1855.
[6] O.V. Boltalina, J. Fluorine Chem. 101 (2000) 273–278.
[7] N.S. Chilingarov, J.V. Rau, L.N. Sidorov, L. Bencze, A. Popovic, V.F. Sukhoverkhov, J. Fluorine Chem. 104 (2000) 291–295.
[8] W. Zhang, K. Guérin, M. Dubois, Z. El Fawal, D.A. Ivanov, L. Vidal, A. Hamwi, Carbon 46 (2008) 1010–1016.
[9] E. Unger, M. Liebau, G.S. Duesberg, A.P. Graham, F. Kreupl, R. Seidel, W. Hoenlein, Chem. Phys. Lett. 399 (2004) 280–283.
[10] J.L. Weeks, C.L. Chernick, M.S. Matheson, J. Am. Chem. Soc. 8 (1962) 4612.
[11] W. Zhang, PhD Thesis, Université Blaise Pascal, Clermont-Ferrand, 2009.
[12] A.M. Panich, Synth. Metals 100 (1999) 169–185.
[13] J. Giraudet, M. Dubois, K. Guérin, C. Delabarre, A. Hamwi, F. Masin, J. Phys. Chem. B 111 (2007) 14143–14151.
[14] T. Mallouk, B.L. Hawkins, M.P. Conrad, K. Zilm, G.E. Maciel, N. Bartlett, Philos. Trans. R. Soc. Lond. A 314 (1985) 179–183.
[15] M. Dubois, J. Giraudet, K. Guérin, A. Hamwi, Z. Fawal, P. Pirotte, F. Masin, J. Phys. Chem. B 110 (2006) 11800–11808.
[16] J. Giraudet, M. Dubois, K. Guérin, C. Delabarre, A. Hamwi, F. Masin, J. Phys. Chem. B 109 (2005) 175–181.
[17] Y. Sato, K. Itoh, R. Hagiwara, T. Fukunaga, Y. Ito, Carbon 42 (2004) 3243–3249.
[18] L. Cai, J.L. Bahr, Y. Yao, J.M. Tour, Chem. Mater. 14 (2002) 4235–4241.
[19] J.M. Simmons, B.M. Nichols, S.E. Baker, M.S. Marcus, O.M. Castellini, C.-S. Lee, R.J. Hamers, M.A. Eriksson, J. Phys. Chem. B 110 (2006) 7113–7118.
[20] D.B. Mawhinney, V. Naumenko, A. Kuznetsova, J.T. Yates, J. Am. Chem. Soc. 122 (2000) 2383–2384.
[21] H. Valdés, M. Sánchez-Polo, J. Rivera-Utrilla, C.A. Zaror, Langmuir 18 (2002) 2111–2116.
[22] O. Byl, J. Liu, J.T. Yates Jr., Langmuir 21 (2005) 4200–4204.
[23] G. McKay, G. McAleavey, Chem. Eng. Res. Des. 66 (1988) 531–536.
[24] C.A. Zaror, J. Chem. Technol. Biotechnol. 70 (1997) 21–28.
[25] J. Rivera-Utrilla, M. Sánchez-Polo, Carbon 40 (2002) 2685–2691.
[26] F. Caturla, J.M. Martínez-Jiménez, M. Molina-Sanio, F. Rodríguez-Reinoso, R. Torregrosa, J. Colloid Interface Sci. 124 (1988) 528–534.
[27] H. Valdés, M. Sanchez-Polo, J. Rivera-Utrilla, C.A. Zaror, Langmuir 18 (2002) 2111–2116.
[28] P.M. Álvarez, J.F. García-Araya, F.J. Beltrán, F.J. Masa, F. Medina, J. Colloid Interface Sci. 283 (2005) 503–512.
[29] W. Zhang, K. Guérin, M. Dubois, A. Houdayer, F. Masin, A. Hamwi, Carbon 46 (2008) 1017–1024.
[30] P. Thomas, D. Himmel, J.L. Mansot, M. Dubois, K. Guérin, W. Zhang, A. Hamwi, Tribol. Lett. 34 (2009) 49–59.
[31] R.L. Fusaro, H.E. Sliney, NASA Tech. Note D-5097, 1969.
[32] C. Martin, J. Sailleau, M. Roussel, Wear 34 (1975) 215.
[33] K. Delbé, P. Thomas, D. Himmel, J.L. Mansot, M. Dubois, K. Guérin, C. Delabarre, A. Hamwi, Tribol. Lett. 37 (2010) 31–41.